Water Research 243 (2023) 120329

Contents lists available at ScienceDirect

Water Research

journal homepage: www.elsevier.com/locate/watres

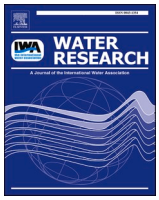

Microplastic and natural sediment in bed load saltation: Material does not dictate the fate

J. Lofty [a], D. Valero [b,c], C.A.M.E. Wilson [a], M.J. Franca [b], P. Ouro [d,*]

[a] School of Engineering, Hydro-Environmental Research Centre, Cardiff University, Cardiff, Wales, UK
[b] Karlsruhe Institute of Technology, Karlsruhe, Germany
[c] IHE Delft, Water Resources and Ecosystems Department, Delft, the Netherlands
[d] School of Engineering, University of Manchester, Manchester, UK

ARTICLE INFO

Keywords:
Plastic transport
Micro plastic
Plastic density
Bedload
Rouse number
River pollution

ABSTRACT

Microplastic (MP) pollution is a well document threat to our aquatic and terrestrial ecosystems, however, the mechanisms by which MPs are transported in river flows are still unknown. The transport of MPs and natural sediment in aquatic flows could be somewhat comparable, as particles are similar in size. However, it is unknown how the lower density of MPs, their shape and their different material properties impact transport dynamics. To answer this, novel laboratory experiments on bed load saltation dynamics in an open-channel flow, using high-speed camera imaging and the detection of 11,035 individual saltation events were used to identify the similarities and differences between spherical MPs and spherical natural sediments transport. The tested MPs and sediment varied in terms of size and material properties (density and elasticity). Our analysis shows that the Rouse number accurately describes saltation length, height, transport velocity and collision angles equally well for both MPs and natural sediments. Through statistical inference, the distribution functions of saltation trajectory characteristics for MPs were analogous to natural sediment with only one sediment experiment (1.4% of cases) differing from all other plastic experiments. Similarly, only nine experiments (9.3% of cases) showed that collision angles for MPs differed from those of natural sediment experiments. Differences observed in terms of restitution become negligible in overall transport dynamics as turbulence overcomes the kinetic energy lost at particle-bed impact, which keeps particle motion independent from impact. Overall, spherical MP particles behave similarly to spherical natural sediments in aquatic environments under the examined experimental conditions. This is significant because there is an established body of knowledge for sediment transport that can serve as a foundation for the study of MP transport.

1. Introduction

Plastic polymers have played an influential role in shaping human activities since the 50s - 70s of the past century (Andrady, 2017; Geyer, 2020) but their widespread use has also resulted in environmental contamination (Napper et al., 2020; Andrade et al., 2021; Lofty et al., 2022). Toxicologists are increasingly concerned about the potential harm caused by plastics to human health (Dick Vethaak and Legler, 2021; Koelmans et al., 2022) and just recently, plastics have been found in human blood (Leslie et al., 2022), lung tissue (Jenner et al., 2022) and even the placenta (Li et al., 2018; Amereh et al., 2022; Ragusa et al., 2022). Plastics can also have detrimental effects to ecosystems on land (Browne et al., 2013; Wu et al., 2022) and water (Kirstein et al., 2016; Galloway et al., 2017; Parker et al., 2021) as particles can be readily ingested by a range of organisms (Cole et al., 2013; Wilcox et al., 2018; D'Souza et al., 2020). In addition, the capacity of plastic particles to act as vectors for pathogens, organic contaminants, and invasive species attached to their surface has triggered global concern (Gregory, 2009; Viršek et al., 2017; Haegerbaeumer et al., 2019).

Plastic in the environment may be transported in air (Materić et al., 2020) or in water (Waldschläger and Schüttrumpf, 2019b; Emmerik and Schwarz, 2020). In the absence of vegetation (Schreyers et al., 2021; Cesarini and Scalici, 2022) or in-channel structures such as a dam or a rack (Honingh et al., 2020; Meijer et al., 2021), a plastic particle in the river may be transported by the flow, however, little is known yet about plastic transport mechanisms (Waldschläger et al., 2022; Lofty et al.,

* Corresponding author.
E-mail address: pablo.ouro@manchester.ac.uk (P. Ouro).

https://doi.org/10.1016/j.watres.2023.120329
Received 25 March 2023; Received in revised form 20 June 2023; Accepted 7 July 2023
Available online 8 July 2023

2023). For instance, Waldschläger and Schüttrumpf (2019b) investigated the critical velocities for microplastic (MP) (plastics < 5 mm in size) entrainment and found significant variation up to 70% from the classic incipient motion Shields number which was formulated for natural sediment. Other studies have focused on the settling and rising velocities of plastic particles of different shapes and sizes (Khatmullina and Isachenko, 2017; Waldschläger and Schüttrumpf, 2019a; Kuizenga et al., 2022), which allow the determination of drag coefficients that determine the particle–flow coupling.

Recently, it has been proposed that MP particles can be suspended in the water column in a similar way as natural sediments (Cowger et al., 2021), which was shown by Valero et al. (2022) for macroplastics (plastics > 5 mm in size) and Born et al. (2023) for nearly spherical MPs. However, there is limited understanding of the behaviour of plastics in bed load transport, where particles move either by rolling/sliding or successive jumps, named saltation (Dey, 2014; Ancey, 2020). This is significant because the prevalence of plastics in bed load transport is comparable to that of surfaced and suspended plastics (Blondel and Buschman, 2022), with up to 80% of plastic found in riverine sediments being negatively buoyant, thus potentially travelling as bed load (Hurley et al., 2018; Mani et al., 2019), and being conveyed differently to positively buoyant plastics, as suggested by Born et al. (2023).

The transport of MPs and natural sediments in riverine environments could be somewhat similar, as the size of MPs are comparable to a range of natural sediments. However, it is unknown how the lower density of MPs, their shape, and their different material properties, such as elasticity, impact their bed load transport dynamics when compared to natural sediment (Waldschläger et al., 2022). In bed load, when a particle impacts with the bed with a given velocity, a portion of its momentum is lost due to restitution, which varies depending on the particle's elastic material properties (Beer et al., 2007). By losing part of the particle's velocity at impact, a different trajectory may be expected after the rebound, for instance, the particle may remain at lower depths or transition from saltation into rolling/sliding modes, potentially resulting in different concentration profiles in bed load. Therefore, a reasonable question may be posed: how will bed load transport of MPs differ when compared to natural sediment transport, for which there is an established body of knowledge available (van Rijn, 1984; Garcia, 2008; Ancey, 2020). In order to explain the comparability between natural sediments and MPs, each of these variables need to be examined separately.

This study comparatively investigates the bed load saltation motion of spherical MPs and spherical natural sediments, which is the dominant mode of bed load transport (Wiberg and Smith, 1987; Sekine and Kikkawa, 1992). The material-depending variables were isolated and their influence on the transport of MPs, in terms of bed load saltation motion, was examined. Three different plastic materials in two sizes were considered, and their transport dynamics in bed load saltation were compared to experiments with amber particles, which possess similar mechanic properties to natural sediments. For direct comparability, MPs and amber were the same shape and size and experiments were undertaken using same flow conditions, methodology and analysis protocols; thus, reducing potential sources of bias. Hydrodynamic experiments were conducted in an open channel flume with controlled discharge and velocity, with discrete particle movement tracked via a high-speed camera to characterise particle behaviour. Therefore, conclusions on differences and similarities between MPs and natural sediments, uniquely from the material comparison perspective, could be drawn.

2. Methods

2.1. Experimental setup

Experiments were conducted in a 10 m long, 0.3 m wide, 0.3 m deep open channel flume with a longitudinal slope of 1/1000 (Fig. 1). Rough sediment beds, made of quartz sand particles glued to plastic boards with thickness of one particle, covered the floor of the flume over the first 6 m of length, thereafter, the flume was floored with a smooth metal plate. Two sets of upstream roughness boards were tested: a first set consisted of uniformly graded sand particles with sand roughness (k_s) of 1.86 mm (based on median particle diameter d_{50}) and geometric standard deviation of the grain size ($\sigma_g = \sqrt{d_{84}/d_{16}}$) of 1.22, while a second set of boards consisted of uniformly graded sand particles with a k_s of 2.76 mm and σ_g of 1.24.

2.2. Flow conditions

Six steady near-uniform flow conditions for the two sets of fixed

Table 1
Details of the hydraulic conditions from experiments including the discharge Q, bed roughness height k_s, flow depth H, depth-averaged velocity V, Reynolds number Re, Froude number F, shear velocity u_* and friction Reynolds number Re*.

Q (l/s)	k_s(mm)	H (m)	V (m/s)	F (-)	Re (-)	u_* (m/s)	Re* (-)
5	1.86	0.060	0.283	0.369	1698	0.0221	39.8
7.5	1.86	0.075	0.339	0.395	2543	0.0257	46.3
10	1.86	0.088	0.386	0.415	3397	0.0276	49.6
12.5	1.86	0.101	0.418	0.420	4222	0.0288	51.9
15	1.86	0.114	0.446	0.422	5084	0.0294	52.9
17.5	1.86	0.127	0.468	0.419	5944	0.0295	53.2
4.8	2.76	0.060	0.272	0.355	1632	0.0238	64.4
7.5	2.76	0.075	0.339	0.395	2543	0.0267	72.3
10	2.76	0.087	0.391	0.423	3402	0.0288	77.8
13	2.76	0.102	0.434	0.434	4427	0.0300	81.2
16	2.76	0.114	0.477	0.451	5438	0.0314	84.8
17.9	2.76	0.122	0.498	0.455	6076	0.0322	87.0

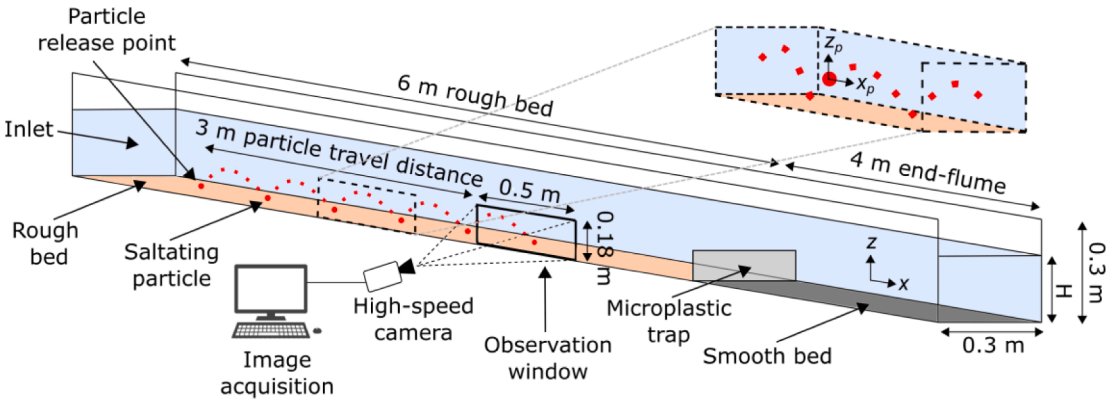

Fig. 1. Experimental setup, instrumentation and particle coordinate system.

roughness beds were established in the flume. Table 1 presents their discharge (Q), flow depth (H), depth-averaged velocity (V), Froude number ($F = V/\sqrt{gH}$), Reynolds number ($Re = VH/\nu$), where ν is the kinematic viscosity of the fluid, shear velocity (u_*) based on the log-law equation and detailed velocity measurements and friction Reynolds number ($Re^* = u_* k_s/\nu$). Flow was recirculated using a pump and measured using an electromagnetic flowmeter (± 0.3%), while the flow depth was controlled by a weir gate. Uniformity of the flow was tested to determine whether channel flow accelerations were negligible and had little influence on the transport of particles.

A two-dimensional particle image velocimetry (PIV) system was used for water velocity measurements in the vertical plane for each of the uniform flow conditions and bed roughnesses. The PIV system employed a high-speed Baumer VLXT-50 M.I camera, able to capture images of 2448 × 2048 px^2 in size at a sampling frequency of 140 frames per second, synced with a stroboscope via a wave generator. The camera was set at 4 m downstream of the flume inlet, in the observation window (Fig. 1) and captured images of 2000 × 700 px^2 (0.50 × 1.85 m^2) in size at a sampling frequency of 120 frames per second for an interval of 30 s. The images were analysed using the MATLAB open-source PIV software, PIVlab (Thielicke and Sonntag, 2021).

The images underwent pre-processing where background subtraction and contrast-limited adaptive histogram equalization (CLAHE) techniques were used of enhance the visibility of particles, while intensity capping and Wiener denoise filtering were used to reduce the error (Thielicke and Sonntag, 2021). Image pairs were correlated by a fast Fourier transform window deformation algorithm where an interrogation window of 128 × 128 pixels was reduced to 32 × 32 pixels with a spatial overlap of 50%. Statistical filtering was used to remove outliers departing far from the median.

The streamwise mean velocity profile was computed through spatial and time averaging. These profiles are presented for all flow conditions in Fig. S1 for completeness. The law of the wall for transitionally rough beds (based on Re^* in Table 1) was fitted to the velocity profiles, allowing the estimation of the shear velocity u_* (Pope, 2000, Eq. 7.121):

$$\frac{u}{u_*} = 5.75\log\left(\frac{z}{k_s}\right) + B \quad (1)$$

where u is the time-averaged streamwise velocity, z is the distance from the bed and B is a constant. The constant B was determined through Fig. 7.24 of Pope (2000), which yielded values of 8.5 for channel beds that were considered hydraulically rough ($Re^* > 70$) and 8.7 for channel beds considered in the hydraulically transitional regime ($Re^* = 30 – 70$). The turbulent boundary layer thickness remained larger than 11.2 mm for $k_s = 1.86$ mm, and 16.7 mm for $k_s = 2.76$ mm, which indicates that the majority of saltation events later presented are within the boundary layer.

2.3. Particle properties

Three plastic materials in two different sizes (3 and 5 mm) were used in the experiments. In order of increasing density, the plastic materials considered were polyamide (PA), cellulose acetate (CA) and polyoxymethylene (POM) which are commonly observed in the riverine environment (Mani et al., 2019; Lenaker et al., 2021; Liu et al., 2021) and are denser than water (1000 kg/m^3), hence susceptible to be transported as bed load. Table 2 presents the properties of the particles used in the experiments with details of their density (ρ_s), settling velocity (W), Young's modulus (E) and Poisson's ratio, defined by Cardaerlli (2008), Grote and Hefazi (2021) and Tkachev et al. (2021).

For comparison, amber particles were also used in the experiments, which have been considered as a proxy for low density natural sediments in riverine transport experiments (Shields, 1936; Rouse, 1939) (Table 2). Table 3 presents the mechanical properties of various natural sediment materials and amber particles. It can be seen that the material properties of amber, such as the Young's modulus (E), which is a key parameter in particle restitution (Melo et al., 2021), is larger than plastics (Table 2), but are analogous common natural sediments formed from rocks (Table 3).

Table 2
Properties of the MP and amber particles used in the experiments including their diameter d, density ρ_s, setting velocity W, Young's modulus E and Poisson's ratio defined by Cardaerlli (2008), Grote and Hefazi (2021), Tkachev et al. (2021).

Particle	d (mm)	ρ_s (± std) (kg/m^3)	W (± std) (m/s)	E (GPa)	Poisson's ratio
PA	3	1104.0 ± 5.9	0.0811 ± 0.0030	2.0	0.38
	5	1107.1 ± 5.2	0.1195 ± 0.0033	2.0	0.38
CA	3	1262.0 ± 15.3	0.1267 ± 0.0043	3.3	0.39 – 0.44
	5	1262.4 ± 7.5	0.1813 ± 0.0045	3.3	0.39 – 0.44
POM	3	1346.5 ± 14.1	0.1456 ± 0.0039	3.0	0.35 – 0.37
	5	1361.7 ± 7.5	0.2136 ± 0.0038	3.0	0.35 – 0.37
Amber	5	1041.3 ± 8.3	0.0717 ± 0.0025	70	0.30

Table 3
Material properties of amber compared to other common natural sediments (Ji et al., 2002; Cardaerlli, 2008).

Sediment type	ρ_s (kg/m^3)	E (GPa)	Poisson's ratio	Mohs hardness
Amber	1050–1090	70	0.30	2 - 2.5
Quartz	2640–2730	56–79	0.10 – 0.22	7
Calcite	2715–2940	72 - 88	0.32	3
Dolomite	2760–2840	70–91	0.10 – 0.35	3 - 4

Despite MPs being observed in many different shapes in the riverine environment (Hurley et al., 2018; Corcoran et al., 2020; Woodward et al., 2021), all particles used in experiments were spherical in shape to isolate the impact that the material-dependant variables have on the transport dynamics of plastic. Particles used in experiments are shown in Fig. 2 against the two rough beds used.

The density (ρ_s) of the MPs and amber were determined by using the immersion method according to DIN 53479 standards (ISO 2019). The

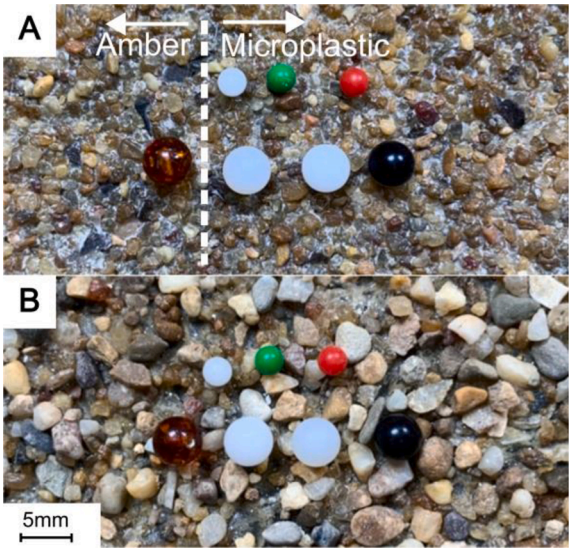

Fig. 2. Photographs of the 5 mm and 3 mm MP and the 5 mm amber particles used in experiments on roughened beds with k_s of (A) 1.86 mm and (B) 2.76 mm.

settling velocity (W) was estimated for all particles, following a similar method to previous studies (Khatmullina and Isachenko, 2017; Waldschläger and Schüttrumpf, 2019a; Jalón-Rojas et al., 2022). A clear cylindrical plexiglass settling column of 1.5 m in height and 0.15 m in diameter was used. The column was filled with distilled water in order to minimise the interaction between the falling particles and other suspended materials in the water. MPs and amber were released by tweezers at the centre of the settling column below the surface of the water to reduce the water surface tension affecting the particles settling velocity. The high-speed camera was used to capture the falling particles at 90 frames per second over a vertical distance of 0.6 m, excluding the upper and lower 0.45 m of the cylinder height to allow the particle to accelerate to terminal velocity. The settling velocity of each MP and amber particle was then calculated as the mean velocity of the falling particle. Each test was repeated five times for each particle.

Given the particle settling velocity (W) and the shear velocity (u_*) for each flow condition, the Rouse number P can be calculated as (Rouse, 1939):

$$P = \frac{W}{\beta \kappa u_*} \tag{2}$$

where $\kappa = 0.41$ is the von Kármán constant and β is a parameter that adjusts the assumption of parabolic eddy diffusive which is assumed to be equal to unity. P determines the shape of the Rouse profile, which is a theoretical concentration profile of particles in turbulent flows and is also used to determine the mode at which particles are transported by the flow. A value of $P > 2.5$ usually indicates a particle is transported as bed load, while a value of P between 0.8 and 2.5 indicates that a particle is in suspended mode of transport (Dey, 2014; Cowger et al., 2021). In this study, Rouse numbers ranged between 5 and 24, which suggests that all particles should predominately be in bed load transport for all flow conditions analysed. For completeness, Shields numbers ranged between 0.027 – 0.512 and Reynolds particle numbers ranged between 66.3 – 161.1 for all flow conditions and particles used.

2.3.1. Experimental procedure

Fig. 1 shows the experimental setup. Between 15 to 20 particles of the same diameter and polymer, for every combination of bed roughness and flow condition (Table 1), were manually released in the upstream region at bed height at the centreline of the flume, one at a time. The particles travel for three meters before moving into the observation window, where the high-speed camera recorded at 90 frames per second captured the motion of the particles with a field of view of 0.5×0.18 m^2. The release point was deemed far enough upstream so that the particle movement captured by the camera was unaffected by the initial conditions or any disturbance developed at the release point, and the particles achieved a steady bed load motion before passing through the observation window. An example video of a 5 mm PA particle moving over a 1.86 mm roughness bed is provided within the supplementary material. At the downstream end of the experimental area, MPs were collected by a sediment trap composed of a mesh sheet (Fig. 1). 11,035 individual saltation events were observed throughout all experiments.

2.4. Video post-processing and saltation characterisation

Video recordings were analysed using open-source software in Fiji (ImageJ2) (Gulyás et al., 2016), where the coordinates (x_p, z_p) of the centroid of the particles moving through the observation window were extracted at each frame of the recorded videos. The coordinates were then used to calculate the mode of particle transport of the particles: rolling/sliding, saltation and suspension. For the saltation events, particle trajectory characteristics and particle–bed collision characteristics were determined. Examples of a 5 mm PA particle trajectory on a 2.76 mm roughness bed, under three different flow condition are shown in Fig. 3 and the different transport modes (rolling/sliding, saltating or suspended transport) are highlighted.

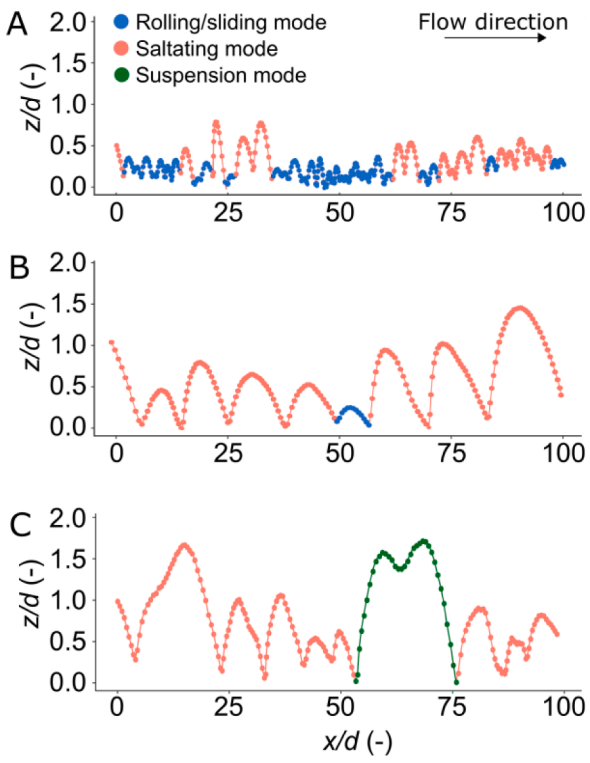

Fig. 3. Trajectories of a 5 mm PA particle travelling over a roughened bed with a k_s of 2.76 mm at increasing shear velocity (A) $u_* = 0.0238$ m/s ($P = 12.5$), (B) $u_* = 0.0288$ m/s ($P = 10.4$) and (C) $u_* = 0.0322$ m/s ($P = 9.27$). Rolling/sliding, saltation and suspension events are highlighted in different colours.

The different modes of particle transport were determined by an algorithm coded in R statistical software (Lofty, 2023) implementing the following algorithm. Looking at a particle, the trajectory from impact to impact with the bed is considered an individual event. Saltation events are events in which the centroid of the particle exceeded a height of k_s/d away from the average height of the sediment bed. If the particle did not reach such heights during the event, then it is classified as rolling/sliding, and involves the particle moving majorly in contact with the bed. Conversely, suspension events were determined as those in which the particle is reverted upwards during the falling limb of the trajectory, i.e., the particle moves upwards again during the falling trajectory and before the collision with the bed (Fig. 3C, green trajectory), which can only be driven by turbulent forces that keep the particle in suspension (Abbott et al., 1977).

To characterise the trajectories of the saltation events in each recording, the saltation length (L_p) was calculated as the distance between two successive saltation collisions with the bed, the saltation height (H_p) was calculated as the maximum height of the saltation event relative to the height of the bed, and the saltation transport velocity (U_p) was calculated as the saltation length divided by the saltation event duration (Fig. 4A). Both L_p and H_p were made dimensionless by the particle diameter d, while U_p was made dimensionless by the shear velocity u^*.

To characterise the collision dynamics, the average inwards (α_{in}) and outwards (α_{out}) collision angles (*prior* and *posterior*), relative to the bed horizontal, were calculated using the x_p, z_p coordinates immediately before and after the particle impact (Fig. 4B). Similarly, the streamwise inwards ($u_p|_{in}$) and outwards ($u_p|_{out}$) velocity and the vertical inwards ($w_p|_{in}$) and outwards ($w_p|_{out}$) velocities were also calculated. The inwards ($v_p|_{in}$) and outwards ($v_p|_{out}$) collision velocity magnitude was calculated as:

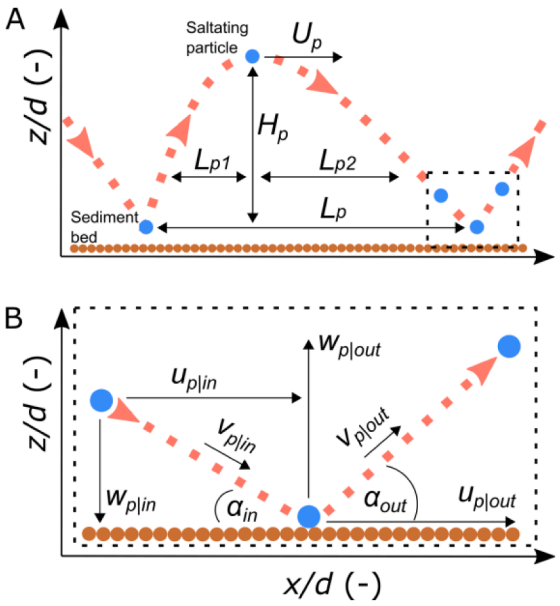

Fig. 4. Definitions of (A) particle trajectory characteristics and (B) particle – bed collision characteristics.

$$v_p|_{in} = \sqrt{u_p|_{in}^2 + w_p|_{in}^2} \tag{3}$$

$$v_p|_{out} = \sqrt{u_p|_{out}^2 + w_p|_{out}^2} \tag{4}$$

Where u_p and w_p are streamwise and vertical velocities of the particles, calculated through central differences.

3. Results and discussion

3.1. Bed load mode of transport

A total of 1665 individual MP and amber particle runs were recorded, with multiple modes of bed load (rolling/sliding and saltation) and suspended load transport observed. Fig. 5 shows the percentage of time that particles spent either in saltation or in rolling/sliding mode of transport. All particles were mobile for all experimental conditions, which meant no particles were in repose, while suspension events remained below 5% for all particles. Given the low correlation between mode of bed load transport and the Rouse number ($R^2 = 0.223$, Fig. S2), a dimensional analysis approach was undertaken to evaluate the relationship between the different physical particle properties (d, ρ_s, W), fluid motion (u_*) and bed properties (k_s) and the percentage of the MP and amber particles transported as bed load. Fig. 5 shows that a dimensionless parameter with the configuration of a modified Rouse number, $k_s\ W/d\ u_*$, which described more consistently the relative frequency of saltation or rolling/sliding modes of transport ($R^2 = 0.817$).

The parameter $k_s\ W/d\ u_*$ encloses two ratios of variables that define the mechanics of bed load transport of plastics: the first, which refers to the Rouse number, (W/u_*) accounts for the relative influence of the particle's settling velocity W to that of turbulence, described by u_*; the second, accounts for how the bed roughness impacts bed load transport dynamics and it is defined by the relative roughness to the size of the particle (k_s/d), similar to conclusions about hiding/exposure effects made by Waldschläger and Schüttrumpf (2019b) for the initiation of motion for MPs.

The improved fit of this parameter suggests that the mode of transport is not only determined by flow and turbulence (Rouse-based considerations) but also by bed roughness and MP particle size. Hence, particles are more likely to saltate as the ratio between the roughness and MPs diameter decreases or as the strength of turbulence acting upon the particle increases. The collapse of transport mode in Fig. 5 for all particles indicates that material properties did not significantly influence this parameter.

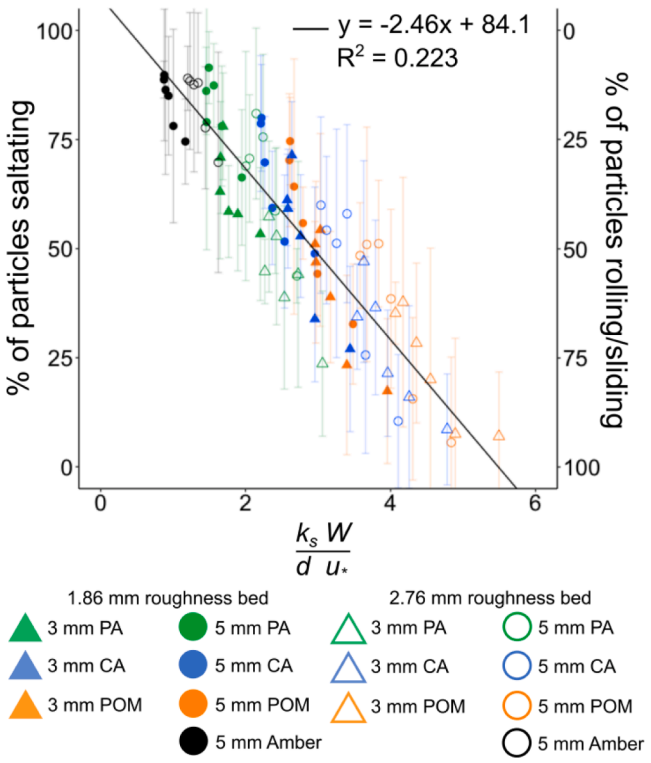

Fig. 5. Percentage of particles in saltation or rolling/sliding mode of transport against a modified Rouse number $k_sW/d\ u_*$, with the solid line indicating a linear fitting. No particles were in repose and less than 5% of all particles were in suspension mode of transport, thus omitted from this analysis.

3.2. Particle trajectory characteristics

Fig. 6A-C shows the main descriptors of the particle trajectories (saltation length L_p, saltation height H_p and saltation transport velocity U_p), which are computed as an average for each material for a certain flow condition and bed roughness. Lower Rouse numbers, indicating higher relative turbulent forces, yielded higher values of L_p, H_p and U_p, suggesting a stronger particle–flow coupling. For the same flow condition, particles with a lower settling velocity (lighter and/or smaller particles) can reach higher regions in the water column with higher velocity, which will accelerate them further; on the other hand, denser and/or larger particles tend to remain closer to the bed. Negligible differences can be seen for values of L_p, H_p and U_p between the two roughness beds, thereby indicating that the k_s/d effect that was not relevant in the trajectory descriptors, as it was in the determination of the permanence of the particles in rolling/sliding or saltating modes as suggested by Fig. 5A.

Fig. 6D – F shows the frequency distribution of L_p, H_p and U_p, considering all individual events for the 5 mm particles of all materials. Frequency distribution plots for the 3 mm MP particles are shown in Fig. S3, for completeness. For each flow condition, the trajectory characteristics are represented through kernel density estimates, which are a nonparametric smoothing alternative to the fitting of a parametric probability density function (Wilks, 2006). It is observed that with decreasing Rouse number, distributions show larger dispersion (also observable in Fig. 6A-C), regardless of the material, likely due to the relatively stronger diffusive effect of turbulence upon the particles'

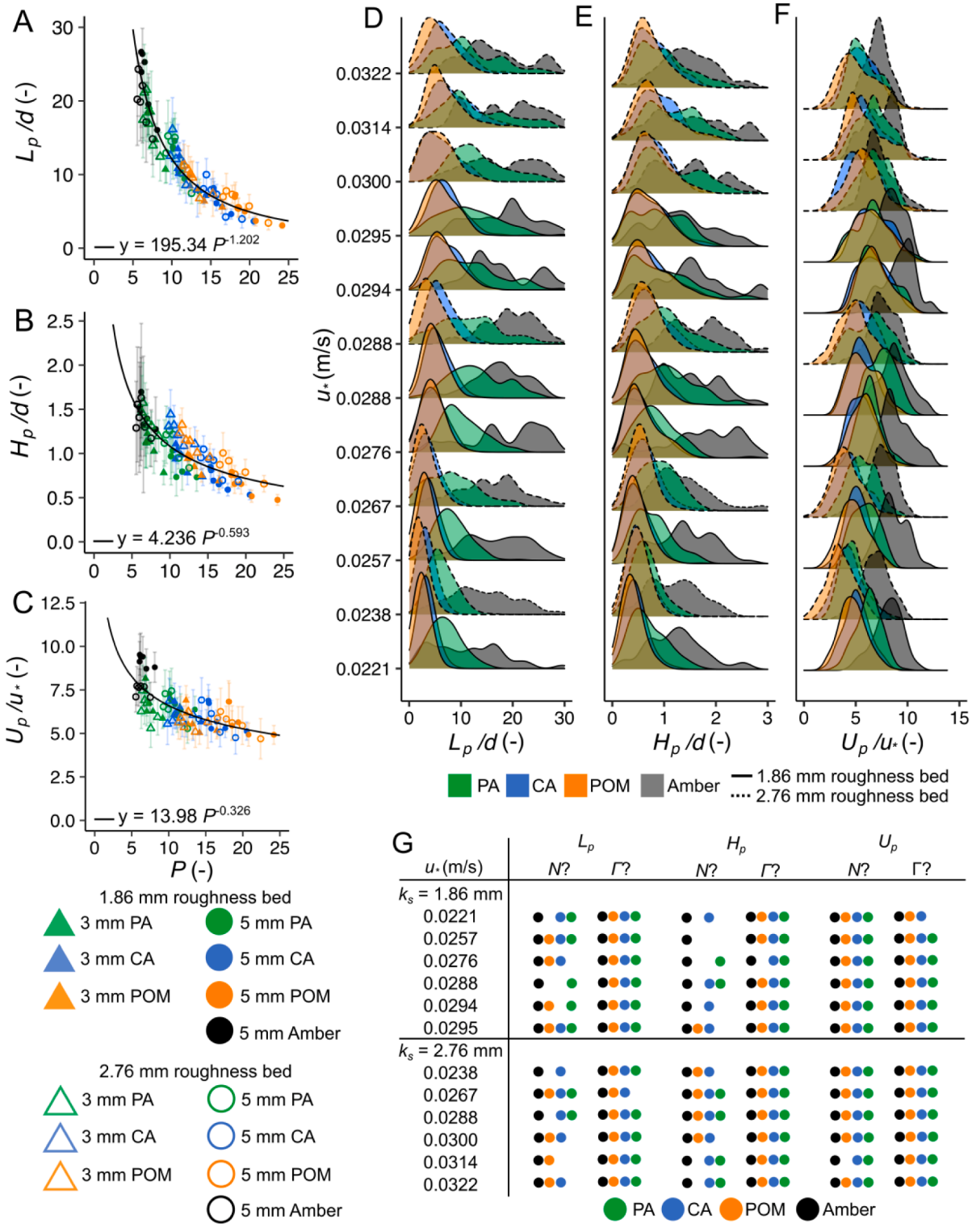

Fig. 6. Average saltation trajectory characteristics, in terms of (A) saltation length L_p, (B) saltation height H_p, and (C) saltation velocity U_p plotted against the Rouse number P. Error bars represent the standard deviation for each material and flow condition. Kernel density plots displaying distribution of 5 mm particles for (D) L_p, (E) H_p, and (F) U_p for each flow condition u_* and bed roughness k_s using a kernel density bandwidth following suggestions of Silverman (1986). (G) Summary of the K-S test indicating where distributions of trajectory characteristics are consistent with a Gaussian (N) and/or Gamma (Γ) functions i.e., $p > 0.05$.

trajectory.

Conversing theories on sediment trajectory probability density functions have been previously proposed; L_p and H_p have both been suggested to fit a Gaussian (Hu and Hui, 1996b) and Gamma (Lee et al., 2000; Lee et al., 2010; Roseberry et al., 2012) distribution, while U_p has been proposed to fit an exponential (Fathel et al., 2015; Shim and Duan, 2019), which is also positively skewed, and Gaussian distributions (Hu and Hui, 1996b; Lee et al., 2000; Lee et al., 2010). In this study, two functions were considered to describe the frequency distributions of L_p, H_p and U_p across particle materials: Gaussian (N), as data may fall

symmetrically around the mean, and Gamma (Γ), to take into consideration the potential skewness, or long tails, that data may show. This may be expected since particle trajectory characteristics should be physically bounded to zero; e.g., no negative saltation jump lengths or heights should be expected.

A one–sample Kolmogorov–Smirnov (K-S) test was performed to identify whether the sampled data is drawn from either a Gaussian or a Gamma function (Wilks, 2006). For that purpose, a Gaussian and a Gamma function are fitted to the data via maximum likelihood estimation. Provided that the probability density functions are identified for MP and amber particles' saltation characteristics, the following question can be addressed: are MPs' trajectories different from those of natural sediments (using amber particles as a proxy)? Fig. 6G compiles the results of the K-S tests for each trajectory characteristic, flow condition, roughness configuration and particle material. Each point in Fig. 6G indicates if the data distribution is consistent with a Gaussian and/or Gamma function ($p > 0.05$).

Fig. 6G can be seen as a similarity matrix in which the points in the same cell indicate that similar probability density functions may be expected for the different particles under the same flow conditions and bed roughness. For instance, considering particle velocity U_p, for the lower k_s bed and a shear velocity of 0.0257 m/s, Gaussian and Gamma distributions can explain the data of all types of particles analogously; however, looking at the distribution of saltation height H_p, we see that only the Gamma function explains this data for all materials, while the Gaussian distribution only explains the amber particles. Altogether, it can be observed that distribution functions of the characteristics from amber experiments were analogous to plastic materials for 85% of all cases, and only one case (1.4%) is different from all the parallel plastic experiments.

From visual inspection of Fig. 6, no apparent difference in behaviour can be observed between MPs and amber particle's trajectory characteristics from an averaged (Fig. 6A-C) or frequency (Fig. 6D-F) point of view. Therefore, a simple model based on P should be able to capture saltation dynamics, regardless of the particle material. Following careful consideration of four regression models (linear, power law, exponential and logarithmic functions), fitted to the data via least squares error minimisation for expected values of L_p, H_p and U_p, it is concluded that a power law function minimised relative bias (Bennett et al., 2013), the most accurate across all materials (Table S1). For completeness, the power law functions are included for Fig. 6A-B.

3.3. Saltation trajectory shape

The shape of the saltation trajectory for particles in bed load is asymmetrical, with the falling limb being larger than the rising limb (Hu and Hui, 1996a; Lee et al., 2000). Results suggest that $L_{p2} \approx 1.5L_{p1}$ and that the ratio of L_{p2}/L_{p1} is independent of the Rouse number, particle material and bed roughness, indicating that the shape of saltation trajectory is alike between MPs and amber particles. The maximum trajectory height (H_p) is roughly 40% of the total trajectory length, which is consistent with previous studies for natural sediment (Hu and Hui, 1996a; Lee et al., 2000).

The shape of the particle saltation trajectories can also be evaluated by identifying the relationship between the average L_p and H_p as shown in Fig. 7A. H_p grew linearly with L_p, with both increasing with decreasing Rouse number. This occurred for both MPs and amber particles. For visualization purposes, Fig. 7B illustrates the trajectory ranges observed for 5 mm MPs and amber particles trajectories, accounting for the average minimum, maximum and values for L_p and H_p. It is seen that the amber particles saltation is longer and higher than the MP particles, which is explained by the larger P values, mainly caused by the smaller settling velocity of the amber particles.

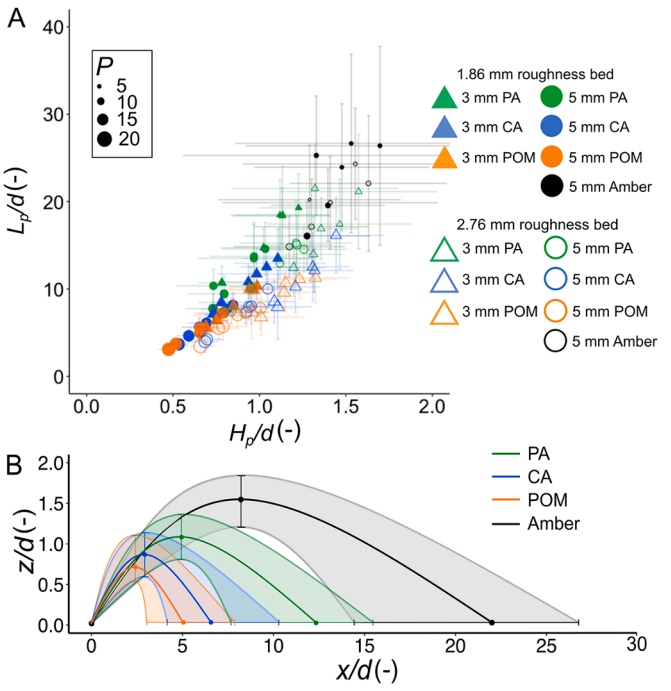

Fig. 7. (A) The average saltation length L_p plotted against saltation height H_p with point size indicating the Rouse number. Error bars represent the standard deviation. (B) Average minimum, maximum and mean experimental trajectory range for 5 mm particles.

3.4. Particle collision characteristics

3.4.1. Collision angles

Particle collision characteristics are key features of particle saltation as they provide information on the energy loss during impact and rebound dynamics (Zeeshan Ali and Dey, 2019; Pähtz et al., 2020). Fig. 8A shows the average inwards collision angle (α_{in}) against the outwards angle (α_{out}) for the MP and amber particles, as defined in Fig. 4. Results indicate that α_{in} ranged from 4.8° to 15.5° whilst values of α_{out} ranged between 12.2° and 32.6° (min – max, for average angles). On average, α_{out} is larger than α_{in} for all particles, flow conditions and bed roughnesses, suggesting that particles are directed upwards after collision.

Fig. 8B–C show the frequency distribution of α_{in} and α_{out} angles for 5 mm particles represented through kernel density estimates, for each flow condition. The distributions show that, α_{out} has larger dispersion compared to α_{in}, likely to be a result of particle impact with a heterogeneous roughened bed, which leads to a wider range of outward angle possibilities. Conversely, α_{in} is mostly a consequence of the shape of the particle trajectory that was found to be relatively uniform across flow conditions (Section 3.3). This difference in distribution between α_{in} and α_{out} angles is similar to results found by previous experimental research for natural sediments (Lee et al., 2000).

A similar analysis to Section 3.2 was undertaken to identify whether sampled α_{in} and α_{out} data is drawn from either a Gaussian or a Gamma function using K-S tests, and if there are differences between probabilistic descriptors of plastic and natural sediments. Fig. 8D compiles the results of the K-S tests for α_{in} and α_{out} for each flow condition and bed roughness, showing where data is consistent with a Gaussian and/or Gamma distribution ($p > 0.05$). The results show that distribution functions of the collision angle from amber experiments were analogous to the plastic materials for 57% of all cases, with only nine cases (9.3%) differing from all comparable plastic experiments.

At lower Rouse numbers, the particle – flow coupling is stronger and a particle reaches higher water levels in the water column, with larger

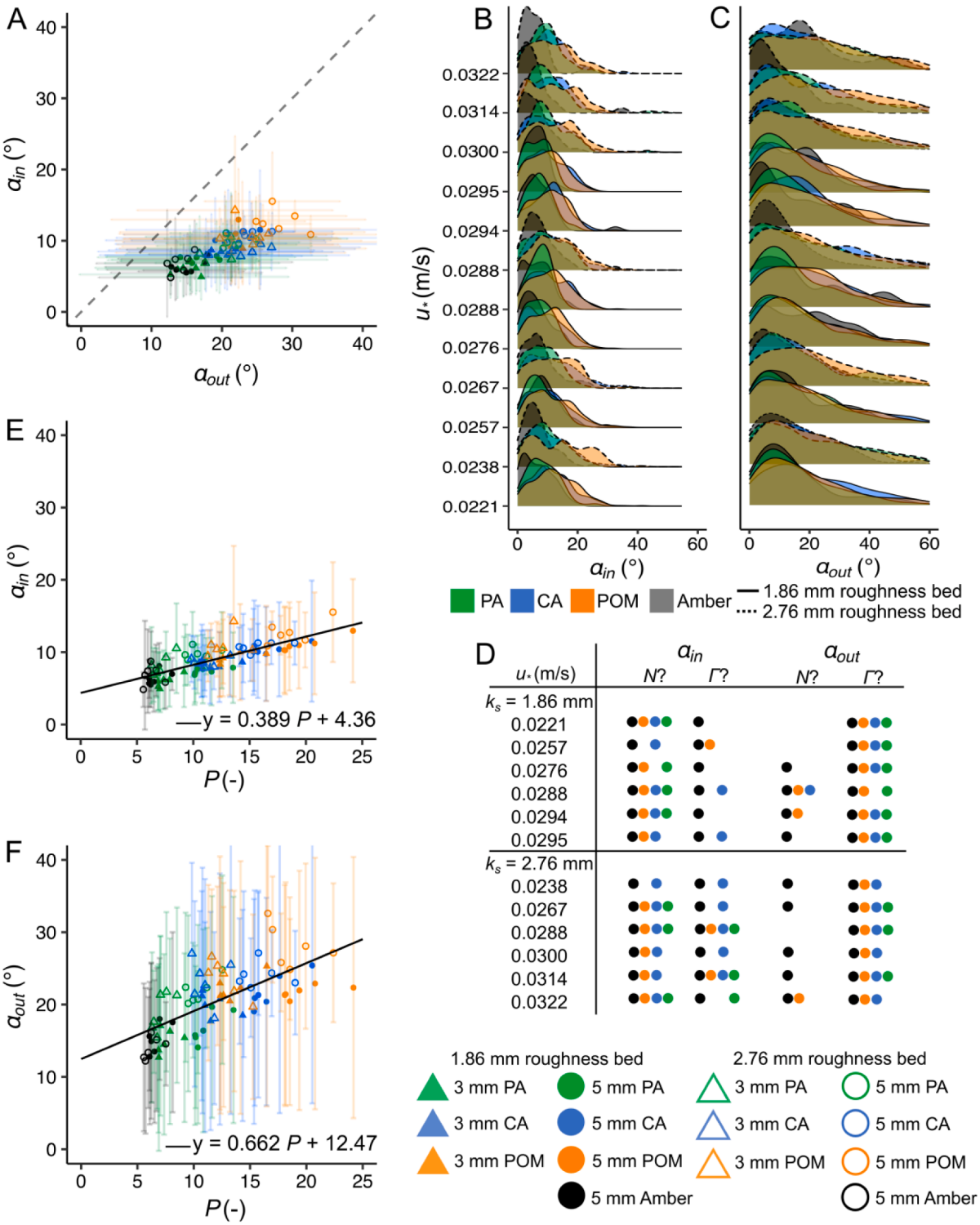

Fig. 8. (A) Inwards collision angle α_{in} plotted against the outwards angle α_{out} and respective kernel density plots for 5 mm particles for (B) α_{in} and (C) α_{out} for each flow condition u_* and bed roughness k_s, using a kernel density bandwidth following suggestions of Silverman (1986). (D) Summary of the K-S test indicating where distributions of α_{in} and α_{out} are consistent with a Gaussian (N) and/or Gamma (Γ) functions i.e., $p > 0.05$. (E) The inwards collision angle α_{in} as a function of the Rouse number P a with fitted linear function. (F) The outwards collision angle α_{out} as a function of the Rouse number P with a fitted linear function.

flow velocities, thus is carried by the flow for a longer distance and this elongates the particle trajectory, causing a flatter α_{in} and α_{out} angles. Based on the observations in Fig. 8E and F, α_{in} and α_{out} appear to be well described by the Rouse number. To quantify their relationship, a linear model is provided that is fitted to the data using least squares error minimisation and keeps relative bias and uncertainty (Bennett et al., 2013) similar across materials (Table S2) and is shown in Fig. 8E-F for completeness.

3.4.2. *Collision velocity*

Fig. 9 shows the average inwards and outwards collision velocities in the streamwise ($u_p|_{in}$, $u_p|_{out}$, Fig. 9A) and vertical directions ($w_p|_{in}$, $w_p|_{out}$,

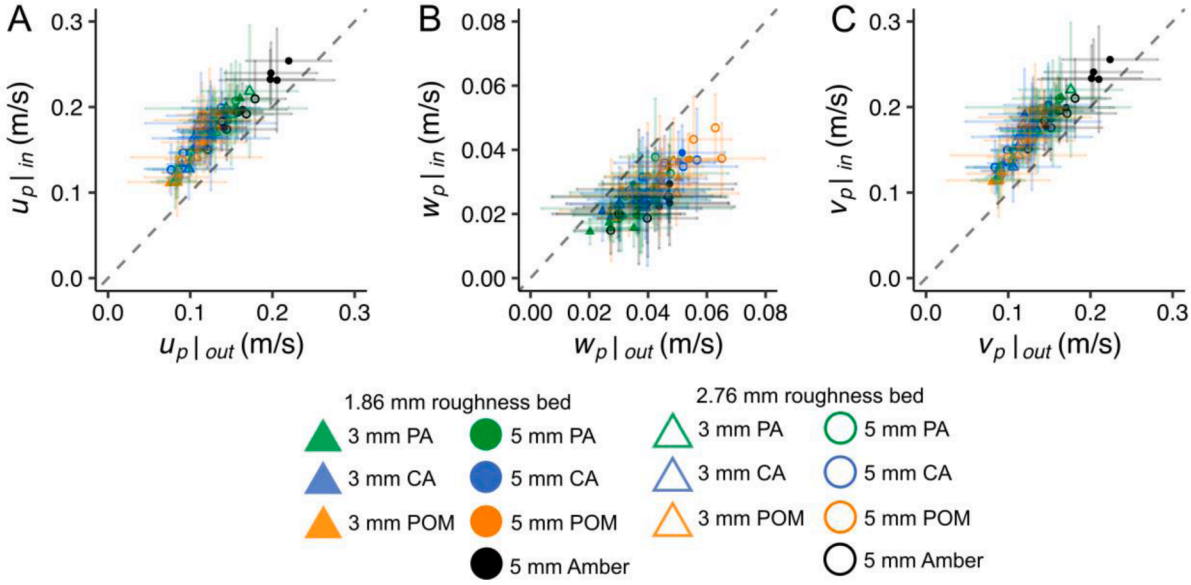

Fig. 9. The average inwards and outwards collision velocities in the (A) streamwise ($u_p|_{in}$, $u_p|_{out}$) and (B) vertical direction ($w_p|_{in}$, $w_p|_{out}$) and (C) the velocity magnitude ($v_p|_{in}$, $v_p|_{out}$).

Fig. 9B), as well as the velocity magnitude ($v_p|_{in}$, $v_p|_{out}$, Fig. 9C). Results show that in the streamwise direction, $u_p|_{in}$ is larger than $u_p|_{out}$ for all particles, while in the vertical direction, $w_p|_{out}$ is larger than $w_p|_{in}$. These results indicate that particles are ejected from collision with a transfer of momentum into the vertical component. During this impact, a part of this energy is dissipated to the bed.

It should be noted that values of $w_p|_{in}$ and $w_p|_{out}$ are a magnitude smaller than values of $u_p|_{in}$ and $u_p|_{out}$, highlighting that the streamwise component dominates the particle's transport and particle–bed collisions. Thus, there is a limited contribution of the vertical velocity component in the calculation of the of $v_p|_{in}$ and $v_p|_{out}$ at collision with the bed. As a result, $v_p|_{in}$ is greater than $v_p|_{out}$, confirming that overall particles move slower after impact with the bed as kinetic energy is lost during collision.

A analysis similar to the one presented in Sections 3.2 and 3.4 was undertaken to identify where observed $u_p|_{in}$, $u_p|_{out}$ and $w_p|_{in}$, $w_p|_{out}$ velocities are possibly drawn from either a Gaussian or a Gamma function using K-S tests, and whether those are different for MPs and natural sediments. For completeness, Fig. S5 shows a compilation of the K-S test results for $u_p|_{in}$, $u_p|_{out}$ and $w_p|_{in}$, $w_p|_{out}$, respectively, showing where data was consistent with a Gaussian and/or Gamma function ($p > 0.05$). The results show that the distribution functions of the collision velocities were analogous to all plastic materials in 90% of cases for $u_p|_{in}$ and $u_p|_{out}$, and 66% of cases for $w_p|_{in}$ and $w_p|_{out}$, with only three cases from all collision velocities (1%) differing from all corresponding plastic experiments.

3.4.3. Restitution coefficient

Provided that part of the inward velocity is lost during the particle-bed impact, it is convenient to define a restitution coefficient (e), which can be also defined in terms of its streamwise (e_x) and vertical (e_z) components:

$$e_x = \frac{u_p|_{out}}{u_p|_{in}} \tag{5}$$

$$e_z = \frac{w_p|_{out}}{w_p|_{in}} \tag{6}$$

$$e = \frac{v_p|_{out}}{v_p|_{in}} \tag{7}$$

The restitution coefficient is directly connected to the loss of kinetic energy during impact (Schmeeckle et al., 2001; Zeeshan Ali and Dey, 2019). Fig. 10 shows the average restitution coefficients by flow condition in A) the streamwise direction e_x, B) vertical direction e_z and C) magnitude e for all particles, plotted against the Rouse number P. Values of e are lower than 1 outlining that kinetic energy is lost during particle-bed collision, while values of e_z are larger than 1, suggesting that kinetic energy is transferred from the streamwise to the vertical direction during collisions, as also indicted by results from the α_{in} and α_{out} collision angles (Fig. 8A). Values of e_x, e_z and e for amber particles are similar to previous studies observations for natural sediment (Hu and Hui, 1996a; Niño and García, 1998).

Results suggest that values of e_x and e for MP particles may be independent of the Rouse number, while values of e_z show a tendency to decrease with increasing Rouse number. It is observed that average values of e_x, e_z and e for PA, CA and POM particles are consistently lower than values for amber particles. An ANOVA statistical test revealed significant differences between values of e_x, e_z and e for the different materials (ANOVA, $p < 0.001$) and a Tukey HSD post hoc confirmed the same findings (amber ~ PA, CA, POM, $p < 0.01$). Overall, these results indicate that the MP particles lose more energy per successive saltation compared to amber particles at impact, which have higher Young's modulus than the MP particles (Table 2) and remain more elastic.

4. Conclusion

This study presents the results of novel laboratory experiments on bed load saltation dynamics using high-speed camera imaging and the detection of 11,035 individual saltation events to identify the similarities and differences between bed load transport dynamics of MPs and natural sediments. Our findings support the following conclusions:

- Saltation trajectory characteristics of MPs are analogous to natural sediments, as distribution functions for MPs were the same as natural sediment with only one amber experiment (1.4% of cases) differing from all other plastic materials (Fig. 6). In all cases, the Rouse parameter could explain saltation length, height and transport velocity equally for all materials tested.
- Inwards and outwards collision angles were well described by the Rouse number, with negligible material influence (Fig. 8). Only nine experiments (9.3% of cases) showed that distribution functions of

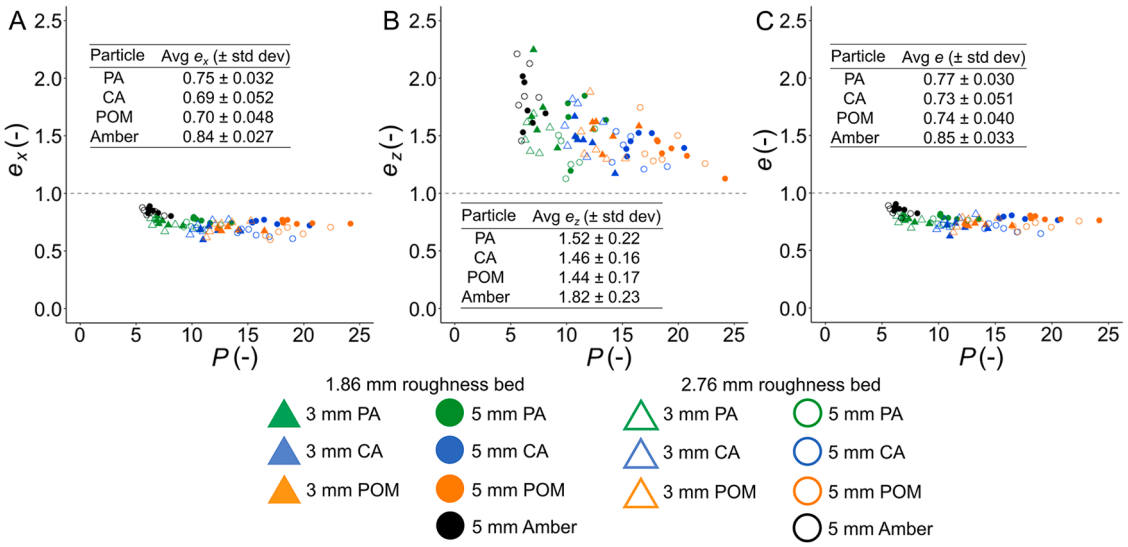

Fig. 10. Restitution coefficients for PA, CA, POM and amber particles for the (A) streamwise e_x, (B) vertical e_z direction and (C) magnitude e.

impact angles for MPs differed from all natural sediment experiments.

- Differences in terms of restitution become negligible in overall transport dynamics as turbulence outweighs the kinetic energy loss during particle-bed collisions and keeps particle motion independent from impact (Fig. 10).

To conclude, spherical MP particles behave similarly to spherical natural sediments in aquatic environments, within experimental uncertainty. Potential differences, due to particle shape will need to be tested separately in future studies since shape-deviations from sediments are significant and have yet to be investigated. The findings of this study are important because there is a well-recognised body of literature in bed load transport (van Rijn, 1984; Garcia, 2008; Ancey, 2020) that can be directly applied to the description of MP transport in rivers within the range of flow conditions herein tested.

CRediT authorship contribution statement

J. Lofty: Conceptualization, Formal analysis, Methodology, Investigation, Visualization, Resources, Software, Writing – original draft, Writing – review & editing. **D. Valero:** Formal analysis, Supervision, Writing – review & editing. **C.A.M.E. Wilson:** Conceptualization, Data curation, Formal analysis, Methodology, Funding acquisition, Project administration, Resources, Supervision, Writing – review & editing. **M. J. Franca:** Formal analysis, Supervision, Writing – review & editing. **P. Ouro:** Conceptualization, Formal analysis, Methodology, Funding acquisition, Project administration, Resources, Supervision, Writing – review & editing.

Declaration of Competing Interest

The authors declare that they have no known competing financial interests or personal relationships that could have appeared to influence the work reported in this paper.

Data availability

Data will be made available on request.

Acknowledgments

This research has been funded by Erasmus+ and the UK Engineering and Physical Sciences Research Council (EPSRC) grant number EP/T517951/1. The authors are grateful to Matthew Moore for the support provided in data analyses.

Supplementary materials

Supplementary material associated with this article can be found, in the online version, at doi:10.1016/j.watres.2023.120329.

References

Abbott, J.E., Francis, J.R.D., Owen, P.R., 1977. Saltation and suspension trajectories of solid grains in a water stream. Philos. Trans. R. Soc. Lond. Ser. A, Math. Phys. Sci. 284 (1321), 225–254. https://doi.org/10.1098/rsta.1977.0009.

Amereh, F., et al., 2022. Placental plastics in young women from general population correlate with reduced foetal growth in IUGR pregnancies. Environ. Pollut. 314, 120174. https://doi.org/10.1016/j.envpol.2022.120174.

Ancey, C., 2020. Bedload transport: a walk between randomness and determinism. Part 1. The state of the art. J. Hydraul. Res. 58, 1–17. https://doi.org/10.1080/00221686.2019.1702594.

Andrade, H., Glüge, J., Herzke, D., Ashta, N.M., Nayagar, S.M., Scheringer, M., 2021. Oceanic long-range transport of organic additives present in plastic products: an overview. Environ. Sci. Eur. 33 (1), 1–14. https://enveurope.springeropen.com/articles/10.1186/s12302-021-00522-x.

Andrady, A.L., 2017. The plastic in microplastics: a review. Mar. Pollut. Bull. 119 (1), 12–22. https://www.sciencedirect.com/science/article/pii/S0025326X1730111X.

Beer, F.P., Johnston, E.R., Clausen, W.E., Cornwell, P.J., Malik, Nilanjan., 2007. Vector Mechanics for Engineers. Dynamics. McGraw-Hill. https://books.google.com/books/about/Vector_Mechanics_for_Engineers.html?hl=sr&id=5emgLAAACAAJ.

Bennett, N.D., et al., 2013. Characterising performance of environmental models. Environ. Model. Softw. 40, 1–20. https://doi.org/10.1016/j.envsoft.2012.09.011.

Blondel, E., Buschman, F.A., 2022. Vertical and horizontal plastic litter distribution in a bend of a Tidal River. Front. Environ. Sci. 10. https://www.frontiersin.org/articles/10.3389/fenvs.2022.861457/full.

Born, M.P., Brüll, C., Schaefer, D., Hillebrand, G., Schüttrumpf, H., 2023. Determination of microplastics' vertical concentration transport (Rouse) profiles in flumes. Environ. Sci. Technol. 57 (14), 5569–5579. https://pubs.acs.org/doi/10.1021/acs.est.2c06885.

Browne, M.A., Niven, S.J., Galloway, T.S., Rowland, S.J., Thompson, R.C., 2013. Microplastic moves pollutants and additives to worms, reducing functions linked to health and biodiversity. Curr. Biol. 23 (23), 2388–2392. http://www.sciencedirect.com/science/article/pii/S0960982213012530.

Cardaerlli, F., 2008. Materials Handbook. Springer London, London. https://doi.org/10.1007/978-1-84628-669-8.

Cesarini, G., Scalici, M., 2022. Riparian vegetation as a trap for plastic litter. Environ. Pollut. 292, 118410 https://doi.org/10.1016/j.envpol.2021.118410.

Cole, M., Lindeque, P., Fileman, E., Halsband, C., Goodhead, R., Moger, J., Galloway, T. S., 2013. Microplastic ingestion by zooplankton. Environ. Sci. Technol. 47 (12), 6646–6655.

Corcoran, P.L., Belontz, S.L., Ryan, K., Walzak, M.J., 2020. Factors controlling the distribution of microplastic particles in benthic sediment of the Thames River, Canada. Environ. Sci. Technol. 54 (2), 818–825.
Cowger, W., Gray, A.B., Guilinger, J.J., Fong, B., Waldschläger, K., 2021. Concentration depth profiles of microplastic particles in river flow and implications for surface sampling. Environ. Sci. Technol. 55 (9), 6032–6041. https://pubs.acs.org/doi/full/10.1021/acs.est.1c01768.
Dey, S., 2014. Fluvial Hydrodynamics. Springer Berlin Heidelberg, Berlin, Heidelberg. https://doi.org/10.1007/978-3-642-19062-9.
Dick Vethaak, A., Legler, J, 2021. Microplastics and human health. Science 371 (6530), 672–674. https://www.science.org/doi/10.1126/science.abe5041.
D'Souza, J.M., Windsor, F.M., Santillo, D., Ormerod, S.J., 2020. Food web transfer of plastics to an apex riverine predator. Glob. Chang Biol. 26 (7), 3846–3857. http://onlinelibrary.wiley.com/doi/abs/10.1111/gcb.15139.
Emmerik, T.v., Schwarz, A., 2020. Plastic debris in rivers. Wiley Interdiscip. Rev. Water 7 (1). http://onlinelibrary.wiley.com/doi/10.1002/wat2.1398.
Fathel, S.L., Furbish, D.J., Schmeeckle, M.W., 2015. Experimental evidence of statistical ensemble behavior in bed load sediment transport. J. Geophys. Res. Earth Surf. 120 (11), 2298–2317. https://doi.org/10.1002/2015JF003552.
Galloway, T.S., Cole, M., Lewis, C., 2017. Interactions of microplastic debris throughout the marine ecosystem. Nat. Ecol. Evol. 1 (5), 1–8. http://www.nature.com/articles/s41559-017-0116.
Garcia, M., 2008. In: Garcia, M. (Ed.), Sedimentation Engineering. American Society of Civil Engineers, Reston, VA.
Geyer, R. 2020. A brief history of plastics. *Mare Plasticum - The Plastic Sea*, pp. 31–47. Available at: https://link.springer.com/chapter/10.1007/978-3-030-38945-1_2.
Gregory, M.R., 2009. Environmental implications of plastic debris in marine settings—entanglement, ingestion, smothering, hangers-on, hitch-hiking and alien invasions. Philos. Trans. R. Soc. B Biol. Sci. 364 (1526), 2013.
Grote, K.H., Hefazi, H., 2021. Springer Handbook of Mechanical Engineering. Springer International Publishing, Cham. https://doi.org/10.1007/978-3-030-47035-7. Grote, KH. and Hefazi, H. eds.
Gulyás, M., Bencsik, N., Pusztai, S., Liliom, H., Schlett, K., 2016. AnimalTracker: an ImageJ-based tracking API to create a customized behaviour analyser program. Neuroinformatics 14 (4), 479–481.
Haegerbaeumer, A., Mueller, M.T., Fueser, H., Traunspurger, W., 2019. Impacts of micro- and nano-sized plastic particles on benthic invertebrates: a literature review and gap analysis. Front. Environ. Sci. 7 (FEB), 17. https://doi.org/10.3389/FENVS.2019.00017/XML/NLM.
Honingh, D., van Emmerik, T., Uijttewaal, W., Kardhana, H., Hoes, O., van de Giesen, N., 2020. Urban river water level increase through plastic waste accumulation at a rack structure. Front. Earth Sci. 8 https://doi.org/10.3389/feart.2020.00028.
Hu, C., Hui, Y., 1996a. Bed-load transport. I: mechanical characteristics. J. Hydraul. Eng. 122 (5), 245–254. https://ascelibrary.org/doi/abs/10.1061/%28ASCE%290733-9429%281996%29122%3A5%28245%29.
Hu, C., Hui, Y., 1996b. Bed-load transport. II: stochastic characteristics. J. Hydraul. Eng. 122 (5), 255–261. https://ascelibrary.org/doi/abs/10.1061/%28ASCE%290733-9429%281996%29122%3A5%28255%29.
Hurley, R., Woodward, J., Rothwell, J.J., 2018. Microplastic contamination of river beds significantly reduced by catchment-wide flooding. Nat. Geosci. 11 (4), 251–257.
ISO. 2019. *ISO - ISO 1183-1:2019 - plastics — methods for determining the density of non-cellular plastics — Part 1: immersion method, liquid pycnometer method and titration method.* Available at: https://www.iso.org/standard/74990.html [Accessed: 10 October 2022].
Jalón-Rojas, I., Romero-Ramírez, A., Fauquembergue, K., Rossignol, L., Me Cachot, J., Sous, D., Morin, B., 2022. Effects of biofilms and particle physical properties on the rising and settling velocities of microplastic fibers and sheets. Environ. Sci. Technol.
Jenner, L.C., Rotchell, J.M., Bennett, R.T., Cowen, M., Tentzeris, V., Sadofsky, L.R., 2022. Detection of microplastics in human lung tissue using μFTIR spectroscopy. Sci. Total Environ. 831, 154907 https://doi.org/10.1016/J.SCITOTENV.2022.154907.
Ji, S., Wang, Q. and Xia, B. 2002. Handbook of seismic properties of minerals, rocks and ores.
Khatmullina, L., Isachenko, I., 2017. Settling velocity of microplastic particles of regular shapes. Mar. Pollut. Bull. 114 (2), 871–880. https://doi.org/10.1016/J.MARPOLBUL.2016.11.024.
Kirstein, I.v, Kirmizi, S., Wichels, A., Garin-Fernandez, A., Erler, R., Löder, M., Gerdts, G., 2016. Dangerous hitchhikers? Evidence for potentially pathogenic Vibrio spp. on microplastic particles. Mar. Environ. Res. 120, 1–8.
Koelmans, A.A., Redondo-Hasselerharm, P.E., Nor, N.H.M., de Ruijter, V.N., Mintenig, S.M., Kooi, M., 2022. Risk assessment of microplastic particles. Nat. Rev. Mater. 7 (2), 138–152.
Kuizenga, B., van Emmerik, T., Waldschläger, K., Kooi, M., 2022. Will it float? Rising and settling velocities of common macroplastic foils. ACS ES T Water 2 (6), 975–981. https://doi.org/10.1021/ACSESTWATER.1C00467.
Lee, H.Y., Chen, Y.H., You, J.Y., Lin, Y.T., 2000. Investigations of continuous bed load saltating process. J. Hydraul. Eng. 126 (9), 691–700. https://doi.org/10.1061/(asce)0733-9429(2000)126:9(691).
Lee, H.Y., Lin, Y.T., You, J.Y., Wang, H.W., 2010. On three-dimensional continuous saltating process of sediment particles near the channel bed. J. Hydraul. Res. 44 (3), 374–389. https://doi.org/10.1080/00221686.2006.9521689.
Lenaker, P.L., Corsi, S.R., Mason, S.A., 2021. Spatial distribution of microplastics in surficial benthic sediment of lake Michigan and Lake Erie. Cite This: Environ. Sci. Technol. 55, 384. https://doi.org/10.1021/acs.est.0c06087.
Leslie, H.A., van Velzen, M.J.M., Brandsma, S.H., Vethaak, A.D., Garcia-Vallejo, J.J., Lamoree, M.H., 2022. Discovery and quantification of plastic particle pollution in human blood. Environ. Int. 163, 107199 https://doi.org/10.1016/J.ENVINT.2022.107199.
Li, J., Zhang, K., Zhang, H., 2018. Adsorption of antibiotics on microplastics. Environ. Pollut. 237, 460–467. https://doi.org/10.1016/J.ENVPOL.2018.02.050.
Liu, S., Chen, H., Wang, J., Su, L., Wang, X., Zhu, J., Lan, W., 2021. The distribution of microplastics in water, sediment, and fish of the Dafeng River, a remote river in China. Ecotoxicol. Environ. Saf. 228, 113009 https://doi.org/10.1016/J.ECOENV.2021.113009.
Lofty, J. 2023. JamesLofty/saltation_microplastic: saltation_microplastic. Available at: https://zenodo.org/record/7763722.
Lofty, J., Muhawenimana, V., Wilson, C.A.M.E., Ouro, P., 2022. Microplastics removal from a primary settler tank in a wastewater treatment plant and estimations of contamination onto European agricultural land via sewage sludge recycling. Environ. Pollut. 304, 119198.
Lofty, J., Ouro, P., Wilson, C.A.M.E., 2023. Microplastics in the riverine environment: meta-analysis and quality criteria for developing robust field sampling procedures. Sci. Total Environ. 863, 160893 https://doi.org/10.1016/j.scitotenv.2022.160893.
Mani, T., Primpke, S., Lorenz, C., Gerdts, G. and Burkhardt-Holm, P. 2019. Microplastic pollution in benthic midstream sediments of the Rhine River.
Materić, D., et al., 2020. Micro- and nanoplastics in alpine snow: a new method for chemical identification and (Semi)quantification in the nanogram range. Environ. Sci. Technol. 54 (4), 2353–2359. https://doi.org/10.1021/acs.est.9b07540.
Meijer, L.J.J., Emmerik, T.van, Ent, R.van der, Schmidt, C., Lebreton, L, 2021. More than 1000 rivers account for 80% of global riverine plastic emissions into the ocean. Sci. Adv. 7 (18) eaaz5803. http://advances.sciencemag.org/content/7/18/eaaz5803.
Melo, K.R.B., de Pádua, T.F., Lopes, G.C., 2021. A coefficient of restitution model for particle–surface collision of particles with a wide range of mechanical characteristics. Adv. Powder Technol. 32 (12), 4723–4733. https://doi.org/10.1016/J.APT.2021.10.023.
Napper, I.E., et al., 2020. Reaching new heights in plastic pollution—preliminary findings of microplastics on Mount Everest. One Earth 3 (5), 621–630. https://doi.org/10.1016/J.ONEEAR.2020.10.020.
Niño, Y., García, M., 1998. Experiments on saltation of sand in water. J. Hydraul. Eng. 124 (10), 1014–1025.
Pähtz, T., Clark, A.H., Valyrakis, M., Durán, O., 2020. The physics of sediment transport initiation, cessation, and entrainment across aeolian and fluvial environments. Rev. Geophys. 58 (1) p. e2019RG000679.
Parker, B., Andreou, D., Green, I.D., Britton, J.R., 2021. Microplastics in freshwater fishes: occurrence, impacts and future perspectives. Fish Fish. 22 (3), 467–488.
Pope, S.B. 2000. Turbulent flows. Available at: https://www.cambridge.org/core/product/identifier/9780511840531/type/book.
Ragusa, A., et al., 2022. Deeply in plasticenta: presence of microplastics in the intracellular compartment of human placentas. Int. J. Environ. Res Public Health 19 (18), 11593.
van Rijn, L.C., 1984. Sediment transport, part i: bed load transport. J. Hydraul. Eng. 110 (10), 1431–1456.
Roseberry, J.C., Schmeeckle, M.W., Furbish, D.J., 2012. A probabilistic description of the bed load sediment flux: 2. Particle activity and motions. J. Geophys. Res. Earth Surf. 117 (F3), 3032.
Rouse, H. 1939. An analysis of sediment transportation in the light of fluid turbulence.
Schmeeckle, M.W., Nelson, J.M., Pitlick, J., Bennett, J.P., 2001. Interparticle collision of natural sediment grains in water. Water Resour. Res. 37 (9), 2377–2391.
Schreyers, L., et al., 2021. Plastic plants: the role of water hyacinths in plastic transport in tropical rivers. Front. Environ. Sci. 9 https://doi.org/10.3389/fenvs.2021.686334.
Sekine, M., Kikkawa, H., 1992. Mechanics of saltating grains. II. J. Hydraul. Eng. 118 (4), 536–558.
Shields, A., 1936. Anwendung der aehnlichkeitsmechanik und der turbulenzforschung auf die geschiebebewegung. PhD Thesis Technical University Berlin.
Shim, J., Duan, J., 2019. Experimental and theoretical study of bed load particle velocity. J. Hydraul. Res. 57 (1), 62–74.
Silverman, B.W., 1986. Density Estimation for Statistics and Data Analysis. Taylor & Francis.
Thielicke, W., Sonntag, R., 2021. Particle image velocimetry for MATLAB: accuracy and enhanced algorithms in PIVlab. J. Open Res. Softw. 9 (1), 1–14.
Tkachev, S.N., Ahart, M., Novikov, V.N., Kojima, S., 2021. Pressure dependence of Poisson's ratio of glassy Baltic amber studied by Brillouin scattering spectroscopy. Jpn. J. Appl. Phys. 60 (SD). SDDA04.
Valero, D., Belay, B.S., Moreno-Rodenas, A., Kramer, M., Franca, M.J., 2022. The key role of surface tension in the transport and quantification of plastic pollution in rivers. Water Res. 226, 119078 https://doi.org/10.1016/j.watres.2022.119078.
Viršek, M.K., Lovšin, M.N., Koren, Š., Kržan, A., Peterlin, M., 2017. Microplastics as a vector for the transport of the bacterial fish pathogen species Aeromonas salmonicida. Mar. Pollut. Bull. 125 (1–2), 301–309.. https://doi.org/10.1016/j.marpolbul.2017.08.024.
Waldschläger, K., et al., 2022. Learning from natural sediments to tackle microplastics challenges: a multidisciplinary perspective. Earth-Sci. Rev. 228, 104021.
Waldschläger, K., Schüttrumpf, H., 2019a. Effects of particle properties on the settling and rise velocities of microplastics in freshwater under laboratory conditions. Environ. Sci. Technology. 53 (4), 1958–1966. https://pubs.acs.org/doi/full/10.1021/acs.est.8b06794.
Waldschläger, K., Schüttrumpf, H., 2019b. Erosion behavior of different microplastic particles in comparison to natural sediments. Environ. Sci. Technol. 53 (22), 13219–13227. https://doi.org/10.1021/acs.est.9b05394.

Wiberg, P.L., Smith, J.D., 1987. Calculations of the critical shear stress for motion of uniform and heterogeneous sediments. Water Resour. Res. 23 (8), 1471–1480. https://doi.org/10.1029/WR023i008p01471.

Wilcox, C., Puckridge, M., Schuyler, Q.A., Townsend, K., Hardesty, B.D., 2018. A quantitative analysis linking sea turtle mortality and plastic debris ingestion. Sci. Rep. 8 (1), 1–11. https://doi.org/10.1038/s41598-018-30038-z.

Wilks, D.S., 2006. Statistical Methods in the Atmospheric Sciences. Elsevier Science.

Woodward, J., Li, J., Rothwell, J., Hurley, R., 2021. Acute riverine microplastic contamination due to avoidable releases of untreated wastewater. Nat. Sustain. 4 (9), 793–802. https://doi.org/10.1038/s41893-021-00718-2.

Wu, X., et al., 2022. Microplastics affect rice (Oryza sativa L.) quality by interfering metabolite accumulation and energy expenditure pathways: a field study. J. Hazard. Mater. 422, 126834 https://doi.org/10.1016/J.JHAZMAT.2021.126834.

Zeeshan Ali, S., Dey, S, 2019. Bed particle saltation in turbulent wall-shear flow: a review. In: Proceedings of the Royal Society A: Mathematical, Physical and Engineering Sciences, 475, p. 20180824. https://doi.org/10.1098/rspa.2018.0824.